Spin-polarized valley Hall effect in ultrathin silicon nanomembrane via interlayer antiferromagnetic coupling

2D Materials

RECEIVED
17 June 2016

REVISED
31 August 2016

ACCEPTED FOR PUBLICATION
1 September 2016

PUBLISHED
14 September 2016

PAPER

Spin-polarized valley Hall effect in ultrathin silicon nanomembrane via interlayer antiferromagnetic coupling

Jia-Tao Sun[1,2], **Zhengfei Wang**[2,3], **S Meng**[1], **Shixuan Du**[1], **F Liu**[2] **and H-J Gao**[1]

[1] Beijing National Laboratory for Condensed Matter Physics and Institute of Physics, Chinese Academy of Sciences, Beijing, 100190, People's Republic of China
[2] Department of Materials Science and Engineering, University of Utah, UT 84112, USA
[3] Hefei National Laboratory for Physical Sciences at the Microscale, University of Science and Technology of China, Hefei, Anhui 230026, People's Republic of China

E-mail: jtsun@iphy.ac.cn

Keywords: silicon nanomembrane, circular photogalvanic effect, layer antiferromagnetic exchange coupling, valleytronics

Supplementary material for this article is available online

Abstract

Fundamental understanding of two-dimensional materials has spurred a surge in the search for topological quantum phase associated with the valley degree of freedom (VDOF). We discuss a spin-polarized version to the VDOF in which spin degeneracy is broken by the antiferromagnetic exchange coupling (LAFM) between opposite layers of the quasi-two-dimensional silicon nanomembrane (SiNM). Based on first principles calculations, we found that the LAFM state in SiNM can lead to metal–insulator transition (MIT). The broken degeneracy of spin degree of freedom in this insulating state of ultrathin SiNM may differ for different valleys, so that the SiNM can be exploited to produce the spatially separated spin and valley currents. We propose that the tunable spin-polarized valley photocurrents can be generated in an experimentally feasible ellipsometry setup. Our work shows promise for the development of spintronic and valleytronic devices compatible with current silicon industry.

Recently the atomically thin two-dimensional transition metal dichalcogenides (TMD) with inversion symmetry breaking have received much research interest because the electrons in solids are endowed with valley pseudospin degree of freedom in addition to real spin. Being able to manipulate the valley pseudospin shows promise for next-generation electronic devices in conventional semiconductors such as valley filter and valve etc [1–7]. The opposite orbital magnetic moments in a pair of nonequivalent valleys in a hexagonal Brillouin zone (BZ) corners underlies the valley-selective circular dichroism (VSCD) [8, 9], the quantum valley Hall effect (QVHE) [10–12], and the valley Zeeman effect etc [13–16]. Since the spin degree of freedom (SDOF) normally mixes with valley analogy, the generation and manipulation of the spatially separated spin current and valley currents remains challenging [17].

Motivated by the promising applications of silicon nanomembrane (SiNM) and particularly the capability of straightforward integration into existing Si-based technology platforms, SiNM was recently assumed to realize potential valley devices [18–26]. Since valley polarization has to be obliged to band gap opening around the Fermi level thanks to the optical excitation [8, 9], the electronically metallic properties [27, 28] of a few monolayer silicon materials however render that the spin-polarized valley currents by optical pumping can not be practically feasible in ultrathin SiNM.

In this work, we propose theoretically by density functional theory calculations that thickness-dependent quantized spin-polarized valley currents could be viable in SiNM. When the antiferromagnetic exchange coupling (LAFM) between the top and bottom layers in ultrathin SiNM is taken into account [29], it leads to the metal–insulator transition (MIT) with an energy gap of 0.29 eV at the mean field theory level. The nonequilibrium charge carriers of valley degree of freedom (VDOF) in SiNM can be realizable in an experimental ellipsometry setup regulated by the optical pumping alike the circular photogalvanic effect (CPGE).

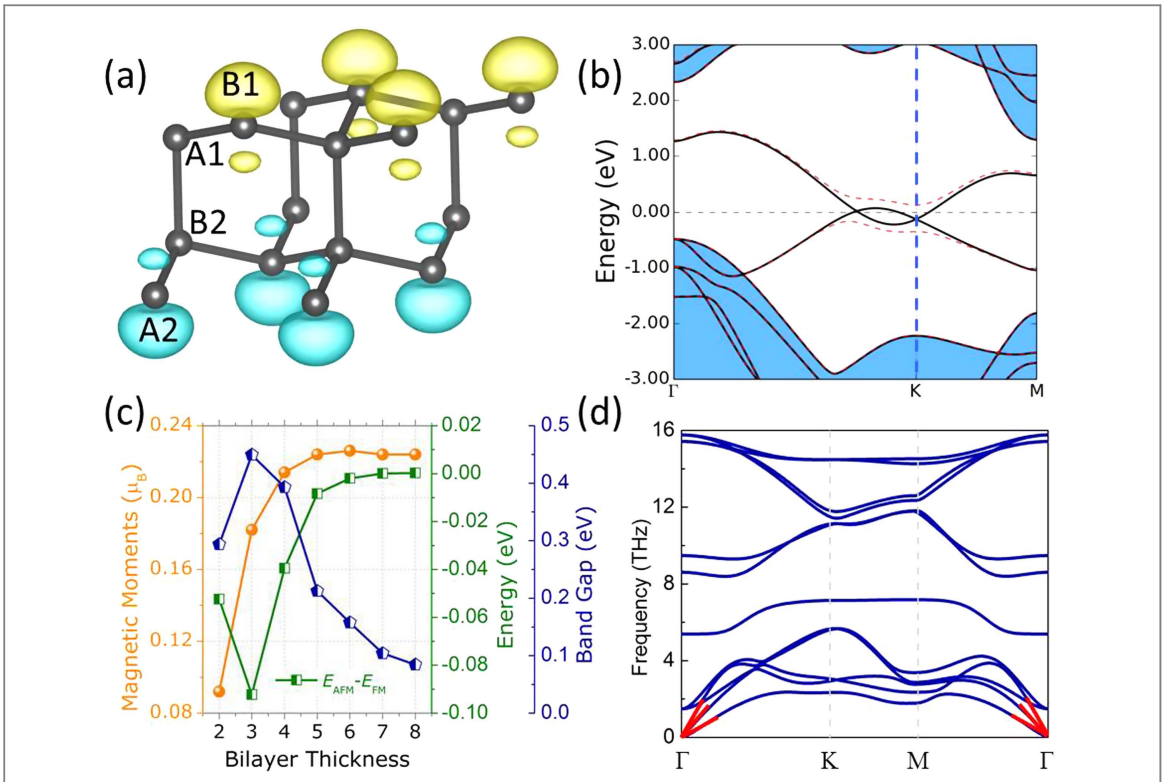

Figure 1. (a) Bernal stacked two-bilayer SiNM structure. The overlapped magnetization density (4×10^{-3} electron Å^{-3}) of the LAFM state is denoted by yellow (blue) color for spin-up (spin-down) electron. (b) Electronic band structures of nonmagnetic state (solid black) and LAFM state (dashed red) of two-bilayer SiNM. (c) Layer dependence of the energy gap (blue), the magnetic moments (orange) for the top-most silicon atom, the energy difference (green) between the LAFM state and the ferromagnetic state. (d) Phonon dispersion of two-layer silicon structure including the layer antiferromagnetic coupling. The acoustic phonons around the Γ point are denoted by solid red lines.

The ultrathin SiNM can be effectively viewed as a multilayer silicene with a Bernal-type stacking as shown in figure 1(a) [25]. The band structure of two-bilayer SiNM in nonmagnetic (NM) state shows that the band dispersion around the nonequivalent K and K′ valley overlap in energy and the band extremum around each valley are shifted with respect to each other in the (k_x, k_y) plane. When the initial magnetized moments were set to the silicon atoms on top and bottom layer of two-bilayer SiNM with opposite sign, the self-consistent calculations leads to a LAFM state, which is more stable by 50 meV than the ferromagnetic (FM) state (figure 1(c)) (for calculation details, see the supplementary information). The calculated band structures of two-bilayer SiNM in LAFM state show that a real global gap of 0.29 eV around the Fermi level is introduced with the anticrossing bands (red dashed line in figure 1(b)) indicating the MIT. The calculated magnetized charge density (figure 1(a)) mainly comes from the partially hybridized p_z orbital of the outmost atoms (B1 and A2 atoms) on opposite surfaces of two-bilayer SiNM. The B1 (A2) and A1 (B2) atoms show magnetic moments of 0.092 (−0.092) μ_B and −0.015 (+0.015) μ_B respectively (figure 1(c)). The calculated phonon dispersion (figure 1(d)) has no imaginary frequency at all momenta, which indicates that the two-bilayer SiNM in LAFM state is dynamically stable. The optical and acoustic branches are well separated with a phonon band gap appearing around 7.5 THz, which might be a useful signature to spectroscopically determine highly stressed SiNM [30].

With the increasing thickness, it is found that the LAFM state in SiNM can persist up to eight-bilayer with the converged magnetic moments of 0.22 μ_B on surface Si atoms (figure 1(c)) as shown by the magnetization density for four-bilayer SiNM (figure S1(a) in the supplementary information). The energy gap initially increases up to three-bilayer SiNM and then decreases to zero asymptotically. Thus the SiNM with layer thickness smaller than eight-bilayer has an in-plane FM coupling and an out-of-plane AFM coupling, whose underlying mechanism calls for further study [31, 32].

In NM state of SiNM, the spin (↓↑) and valley (K and K′) degree of freedom have quartic degeneracy. When the time reversal symmetry is broken, the LAFM ordering lifts the quartic degeneracy into four distinct states, ↑K, ↑K′, ↓K, ↓K′. Thus, it is quite natural to ask whether it is possible to achieve spin-polarized valley currents in the ultrathin SiNM. In the LAFM state, a translation between top and bottom surface of SiNM is equivalent to reversing the two spin flavors. Although no requirement of inversion symmetry conservation has to be satisfied in the LAFM

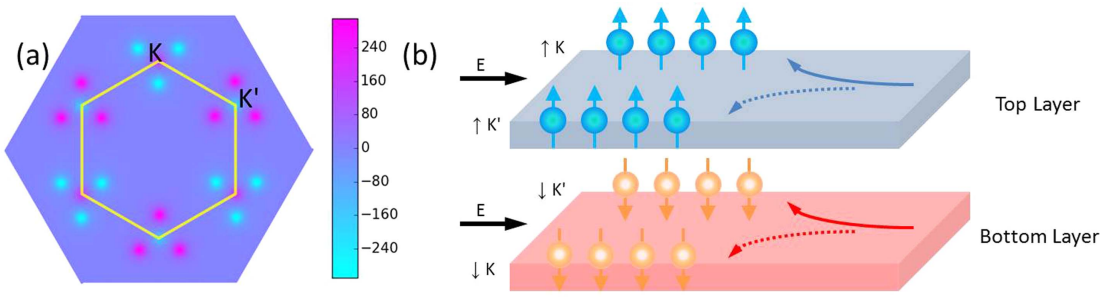

Figure 2. (a) Momentum resolved Berry curvature $\Omega_{\uparrow}(k)$ ($\gamma = 1, \theta = \pi/2$) of direct interband transition between VB and CB in antiferromagnetic two-layer silicon. The first Brillouin zone is denoted by the yellow hexagon. The color code is in atomic units (bohrs^2). (b) Schematic diagram of valley currents in two spin components separated in the top and bottom layer with the presence of in-plane electric field and non-zero Berry curvature.

state, the band gap opening around nonequivalent valley points has to be associated with the separate surface plane. Thus it is obvious that $\Omega_{K\uparrow} = -\Omega_{K\downarrow}$ and $\Omega_{K'\uparrow} = -\Omega_{K'\downarrow}$, where $\Omega_{K\uparrow}$ represents the Berry curvature for spin-up $\uparrow$ channel around the valley K point. As a result, LAFM state can provide a versatile playground for realizing the valley and spin currents in SiNM without the requirement for inversion symmetry breaking as the VSCD in TMDs materials [8, 33, 34].

According to the semiclassical equations of motion $v(k) = \frac{1}{\hbar}\frac{\partial \varepsilon(k)}{\partial k} + \frac{e}{\hbar}\boldsymbol{E} \times \Omega(k)$, the intrinsic anomalous Hall conductivity σ_{xy} of the occupied manifolds reads as [35, 36]

$$\sigma_{xy} = \pm\mathbb{C}\frac{e^2}{h} = \frac{e^2}{2\pi h}\int \mathrm{d}^2k\Omega(k), \qquad (1)$$

where $\mathbb{C}$ stands for the first Chern number. The momentum dependence of Berry curvature $\Omega(k)$ (the spin index is ignored here for simplicity) is obtained by [33]

$$\Omega(k) = -\frac{\hbar^2}{m^2}\sum_{i\neq j}\frac{|\mathcal{P}_{ij}^{+}(k)|^2 - |\mathcal{P}_{ij}^{-}(k)|^2}{[\varepsilon_i - \epsilon_j]^2}, \qquad (2)$$

where $\mathcal{P}_{ij}^{\pm}(k) = \mathcal{P}_{ij}^{x}(k) + \gamma e^{\pm i\theta}\mathcal{P}_{ij}^{y}(k)$ stands for the matrix element of light–mater interaction. The index i and j denote the different band index. The helicity of incident light is determined by the amplitude ratio γ and phase retardation θ. $\gamma = 1$ ($\gamma \neq 1$) corresponds to circular (ellipsometric) polarized light. The direct interband transition matrix $\mathcal{P}_{ij}^{\alpha}(\boldsymbol{\kappa}) = -i\hbar\langle u_j(\boldsymbol{k})|\nabla_{\alpha}|u_i(\boldsymbol{k})\rangle$ can be obtained by the density functional perturbation theory. For the direct interband transition between the top valence band and the bottom conduction band, the momentum dependent berry curvature $\Omega(k)$ (equation (2)) is shown in figure 2(a). Since $\Omega(k)$ is an odd function with respect to the spin flavor $\Omega_{\uparrow K} = \Omega_{\downarrow K'}$, only spin-up flavor of Berry curvature $\Omega_{\uparrow}(k)$ ($\gamma = 1$, $\theta = \pi/2$) is shown in figure 2(a). Valley contrasting Berry curvature in the BZ indicates that in the presence of in-plane electric field, spin-up flavor will acquire anomalous velocities of opposite signs in the two valleys accumulating separately on top surface of silicon nanomembrane yielding spin-polarized QVHE (figure 2(b)). If the integral of the momentum dependent Berry curvature was performed on a closed manifold, say the half BZ (K or K′ valley), we obtained the valley Chern number as $\mathbb{C}_v = 1$ indicating that the single channel long-lived valley currents can persist over extended distances in the absence of spin flip and interlayer scattering. In the presence of in-plane electric-field the population of SDOF of electrons is spatially separated from those of valley counterpart allowing the simultaneous manipulation of spatially separated spin and VDOF without interference in SiNM (figure 2(b)). This has important difference with the previous work [34], where the antiferromagnetic coupling is involved through in-plane nearest-neighbors exchange interaction. However interlayer AFM coupling discussed here simply breaks the quartic degeneracy and do not involve the spin-valley coupled physics as illustrated before.

In order to check the valley-dependent polarization in thicker SiNM, we have calculated the Berry curvature $\Omega_{\uparrow}(k)$ of four-bilayer SiNM for direct interband optical transition of one spin flavor between top of valence band and bottom of conduction band (see the figure S1 in the ESM). It is found that the valley contrasting Berry curvature can still be readily identified in thicker SiNM with smaller triangle spots in the BZ. At equilibrium, the charge carriers' anomalous velocities acquire opposite signs for each spin and valley in freestanding SiNM, exactly canceling each other's contribution to the transverse current. However, the optical absorption is not zero at the valley point from the direct interband transition matrix (equation (2)). This inspired us to selectively excite electrons at the K (K′) valley point by left- (right-) polarized light.

The chiral optical selection rule is determined by both intracellular (parent atomic orbitals) and intercellular (lattice symmetry) current circulation [34]. Due to the weak spin–orbit coupling of p_z orbit of silicon atom, the former part of orbital magnetic moment

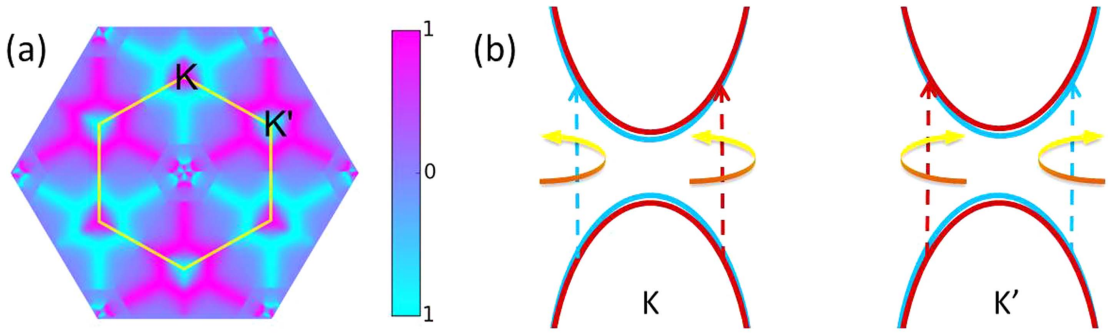

Figure 3. (a) Momentum resolved circular dichroism $\eta(k)$ ($\gamma = 1, \theta = \pi/2$) of two-bilayer silicon nanomembrane for spin-up state in the entire momentum space due to the direct interband transition between VB and CB. The first Brillouin zone is located inside the yellow hexagon. Only the spin up component is plotted, while the other spin component have opposite values in the entire Brillouin zone. (b) Optical transition selection rules of layer spin and valley. The red (blue) colors indicate spin ↑ (↓) components which are shifted slightly for clarity.

is assumed to be absent. The latter part is related to QVHE due to the valley orbital magnetic moments [10]. On this basis, the momentum dependence of circular polarization were calculated via the direct interband dipole transition matrix $\mathcal{P}^{ij}_{\alpha}(k)$ as

$$\eta(k) = \frac{|\mathcal{P}^{+}_{ij}(k)|^2 - |\mathcal{P}^{-}_{ij}(k)|^2}{|\mathcal{P}^{+}_{ij}(k)|^2 + |\mathcal{P}^{+}_{ij}(k)|^2}. \quad (3)$$

This quantity is the difference between the absorption of the left- and right-handed lights, normalized by the total absorption in the momentum space. The calculated degree of circular polarization $\eta(k)$ for spin-up flavor of two-bilayer SiNM shows a three-fold symmetry in the vicinity of K (K′) valley points in figure 3(a). It is clear that the valley contrasting circular dichroism is generated by the circularly polarized light.

The emergence of valley contrasting circular polarization of SiNM in LAFM state allows for the selective generation of nonequilibrium spin and valley carriers by different helicity of incident photon as shown in figure 3(b). The left circularly polarized light (σ^+) can generate a pair of spin ↑ electron and spin ↓ hole in K valley on the top surface. Since the spin angular momentum is conserved in optical transition, σ^+ excitation also generates a pair of spin ↓ electron and spin ↑ hole on the bottom surface. With a sufficiently large in-plane electric field, the pair of spin ↑ electron and spin ↓ hole is dissociated to pile up on the opposite boundary with imbalanced spin Hall currents on the top surface. For the right circularly polarized light (σ^-) excitation, the SHE will behave in a similar way with σ^+ excitation. These results validate the VSCD in SiNM with LAFM state.

If the amplitude ratio $\gamma = 1$ and the phase retardation θ of incident light are applied to the SiNM at the same time in experimental ellipsometric setup, tunable valley current could be feasible. To show this, the valley Chern number is calculated by changing the phase retardation θ from 0 to π and the amplitude ratio γ from 10^{-2} to 10^{2} at an interval of one order. The obtained valley Chern number dependence on the incident light is shown in figure 4. It is seen that the dependence of valley Chern number on the phase retardation θ of the incident light agrees with the standard sine function. In this way the tunable valley current J_{CPGE} from the anomalous transverse velocities (equation (1)) can be generated by circularly polarized lights resulting into CPGE (figure 4(a)). The larger (smaller) amplitude ratio γ of incident light will increase (decrease) the valley current J_{CPGE}. The maximum valley current J_{CPGE} ($\theta = \pi/2$) decrease linearly with the increasing the layer thickness (figure 4(b)) indicating that the larger AFM coupling can enhance the CPGE like the case of two-bilayer SiNM. Thus the tunable spin-polarized quantum valley hall effect might be realized in ellipsometry setup (figure 4(c)) which depends not only on the light helicity but the phase retardation θ and the amplitude ratio γ of incidence light.

In conclusion, we show here that ultrathin pristine SiNM show promising properties of VSCD because two inter-band transitions around the Fermi level are associated with not only the SDOF but also the VDOF. Since spin and valley degeneracy is broken, this leads to spin and valley separation, demonstrating a photo-helicity driven spin and valley current effect [37, 38], which will be beneficial to the spin-optoelectronics for silicon materials. Since the crucial layered spin-polarization in SiNM can have exchange coupling in a layer-separation range of beyond the thickness of several bilayer, the experimental setup can be built by two layer of Dirac system (like graphene and silicene) intercalated by an thin insulating layer, say boron nitride. In this case, the LAFM exchange coupling should remain. Once the layered spin-polarization in van der Waals structures can be measured in experiments by, say spin-polarized scanning tunneling microscopy, our proposal will be promising to be realized under extremely low temperature.

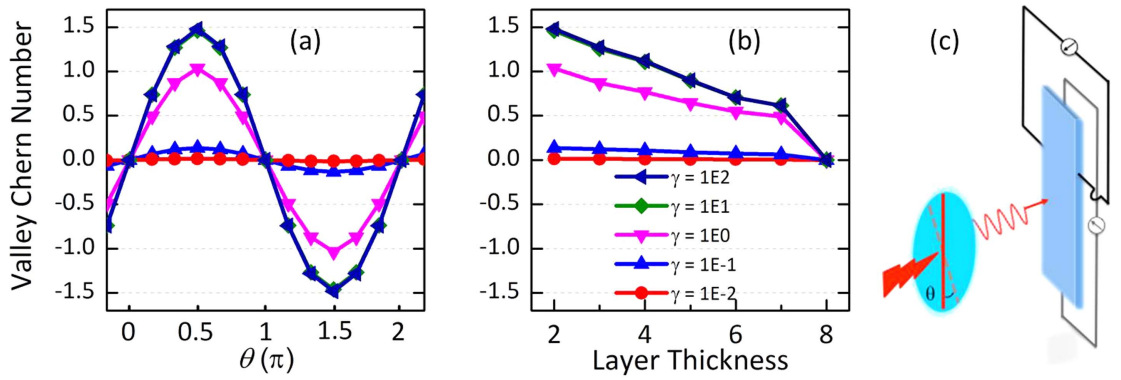

Figure 4. (a) The valley Chern number dependence on the phase retardation θ of the incident light in two-bilayer SiNM when the amplitude ratio γ is varied. (b) The valley Chern number dependence on the SiNM thickness when the phase retardation θ of the incident light is fixed to $\pi/2$.

Acknowledgments

This work was supported by the National Basic Research Program of China (Grant No. 2013CBA01600), the Natural Science Foundation of China (Grant No. 61306114) and 'Strategic Priority Research Program (B)' of the Chinese Academy of Sciences (Grant No. XDB07030100), Chinese Youth 1000 Talents Program.

References

[1] Rycerz A, Tworzydlo J and Beenakker C W J 2007 Valley filter and valley valve in graphene *Nat. Phys.* **3** 172–5
[2] Gunlycke D and White C T 2011 Graphene valley filter using a line defect *Phy. Rev. Lett.* **106** 136806
[3] Isberg J, Gabrysch M, Hammersberg J, Majdi S, Kovi K K and Twitchen D J 2013 Generation, transport and detection of valley-polarized electrons in diamond *Nat. Mater.* **12** 760–4
[4] Zhu Z, Collaudin A, Fauque B, Kang W and Behnia K 2012 Field-induced polarization of dirac valleys in bismuth *Nat. Phys.* **8** 89–94
[5] Gunawan O, Shkolnikov Y P, Vakili K, Gokmen T, DePoortere E P and Shayegan M 2006 Valley susceptibility of an interacting two-dimensional electron system *Phys. Rev. Lett.* **97** 186404
[6] Xiao D, Yao W and Niu Q 2007 Valley-contrasting physics in graphene: magnetic moment and topological transport *Phys. Rev. Lett.* **99** 236809
[7] Xiao D, Chang M C and Niu Q 2010 Berry phase effects on electronic properties *Rev. Mod. Phys.* **82** 1959–2007
[8] Cao T *et al* 2012 Valley-selective circular dichroism of monolayer molybdenum disulphide *Nat. Commun.* **3** 887
[9] Zeng H, Dai J, Yao W, Xiao D and Cui X 2012 Valley polarization in MoS_2 monolayers by optical pumping *Nat. Nano* **7** 490–3
[10] Xiao D, Liu G B, Feng W, Xu X and Yao W 2012 Coupled spin and valley physics in monolayers of MoS_2 and other group-VI dichalcogenides *Phys. Rev. Lett.* **108** 196802
[11] Mak K F, He K, Shan J and Heinz T F 2012 Control of valley polarization in monolayer MoS_2 by optical helicity *Nat. Nano* **7** 494–8
[12] Mak K F, McGill K L, Park J and McEuen P L 2014 Single-electron transport in ropes of carbon nanotubes *Science* **344** 1489–92
[13] Srivastava A, Sidler M, Allain A V, Lembke D S, Kis A and Imamoğlu A 2015 Valley zeeman effect in elementary optical excitations of monolayerWSe_2 *Nat. Phys.* **11** 141–7
[14] Aivazian G, Gong Z, Jones A M, Chu R L, Yan J, Mandrus D G, Zhang C, Cobden D, Yao W and Xu X 2015 Magnetic control of valley pseudospin in monolayer WSe_2 *Nat. Phys.* **11** 148–52
[15] MacNeill D, Heikes C, Mak K F, Anderson Z, Kormányos A, Zólyomi V, Park J and Ralph D C 2015 Breaking of valley degeneracy by magnetic field in monolayer $MoSe_2$ *Phys. Rev. Lett.* **114** 037401
[16] Jones A M *et al* 2013 Optical generation of excitonic valley coherence in monolayer WSe_2 *Nat. Nano* **8** 634–8
[17] Wang Z F, Jin S and Liu F 2013 Spatially separated spin carriers in spin-semiconducting graphene nanoribbons *Phys. Rev. Lett.* **111** 096803
[18] Hwang S W *et al* 2014 Dissolution chemistry and biocompatibility of single-crystalline silicon nanomembranes and associated materials for transient electronics *ACS Nano* **8** 5843–51
[19] Jungwirth T, Wunderlich J, Novák V, Olejník K, Gallagher B L, Campion R P, Edmonds K W, Rushforth A W, Ferguson A J and Němec P 2014 Theory of ferromagnetic (III, Mn)V semiconductors *Rev. Mod. Phys.* **86** 855
[20] Ji H X, Wu X L, Fan L Z, Krien C, Fiering I, Guo Y G, Mei Y and Schmidt O G 2010 Self-wound composite nanomembranes as electrode materials for lithium ion batteries *Adv. Mater.* **22** 4591–5
[21] Bof Bufon C C, Cojal González J D, Thurmer D J, Grimm D, Bauer M and Schmidt O G 2010 Self-assembled ultra-compact energy storage elements based on hybrid nanomembranes *Nano Lett.* **10** 2506–10
[22] Grimm D, Bof Bufon C C, Deneke C, Atkinson P, Thurmer D J, Schäffel F, Gorantla S, Bachmatiuk A and Schmidt O G 2013 Rolled-up nanomembranes as compact 3D architectures for field effect transistors and fluidic sensing applications *Nano Lett.* **13** 213–8
[23] Mei Y, Solovev A A, Sanchez S and Schmidt O G 2011 Rolled-up nanotech on polymers: from basic perception to self-propelled catalytic microengines *Chem. Soc. Rev.* **40** 2109–19
[24] Ying M, Bonifas A P, Lu N, Su Y, Li R, Cheng H, Ameen A, Huang Y and Rogers J A 2012 Silicon nanomembranes for fingertip electronics *Nanotechnology* **23** 344004
[25] Liu F, Liu C C, Wu K, Yang F and Yao Y 2013 $d + id'$ Chiral superconductivity in bilayer silicene *Phys. Rev. Lett.* **111** 066804
[26] Zhou M, Liu Z, Wang Z, Bai Z, Feng Y, Lagally M G and Liu F 2013 Strain-engineered surface transport in Si(001): complete isolation of the surface state via tensile strain *Phys. Rev. Lett.* **111** 246801
[27] Liu C C, Feng W and Yao Y 2011 Quantum spin hall effect in silicene and two-dimensional germanium *Phys. Rev. Lett.* **107** 076802

[28] Cahangirov S, Topsakal M, Aktürk E, Şahin H and Ciraci S 2009 Two- and one-dimensional honeycomb structures of silicon and germanium *Phys. Rev. Lett.* **102** 236804
[29] Xu X, Yao W, Xiao D and Heinz T F 2014 Spin and pseudospins in layered transition metal dichalcogenides *Nat. Phys.* **10** 343–50
[30] Liu F, Ming P and Li J 2007 Ab-initio calculation of ideal strength and phonon instability of graphene under tension *Phys. Rev.* B **76** 064120
[31] Son Y W, Cohen M L and Louie S G 2006 Half-metallic graphene nanoribbons *Nature* **444** 347–9
[32] Jung J, Pereg-Barnea T and MacDonald A H 2009 Theory of interedge superexchange in zigzag edge magnetism *Phys. Rev. Lett.* **102** 227205
[33] Yao W, Xiao D and Niu Q 2008 Valley-dependent optoelectronics from inversion symmetry breaking *Phys. Rev.* B **77** 235406
[34] Li X, Cao T, Niu Q, Shi J and Feng J 2013 Coupling the valley degree of freedom to antiferromagnetic order *Proc. Natl Acad. Sci. USA* **110** 3738–42
[35] Berry M V 1984 Quantal phase factors accompanying adiabatic changes *Proc. R. Soc.* A **392** 45–57
[36] Sundaram G and Niu Q 1999 Wave-packet dynamics in slowly perturbed crystals: gradient corrections and berry-phase effects *Phys. Rev.* B **59** 14915
[37] Ganichev S D, Ivchenko E L, Danilov S N, Eroms J, Wegscheider W, Weiss D and Prettl W 2001 Conversion of spin into directed electric current in quantum wells *Phys. Rev. Lett.* **86** 4358
[38] Hübner J, Rühle W W, Klude M, Hommel D, Bhat R D R, Sipe J E and van Driel H M 2003 Direct observation of optically injected spin-polarized currents in semiconductors *Phys. Rev. Lett.* **90** 216601